Data
Models
Inventories

PARIS

Process Attribution of Regional Emissions

GA 101081430, RIA

EYE-CLIMA

Verifying Emissions of Climate Forcers

GA 101081395, RIA

Preliminary emissions of BC for Europe

This is a joint deliverable of PARIS and EYE-CLIMA (in PARIS, D7.4 and in EYE-CLIMA, D3.8).

D7.4 (PARIS) | D3.8 (EYE-CLIMA)			
Delivery due date Annex I	31 Dez. 2024		
Actual date of submission	7 Feb. 2025		
Lead beneficiary: UNIURB	Work package: 7	Nature: Report	Dissemination level: PU
Responsible scientist	S. Annadate, UNIURB		
Contributors	PARIS: E. Mancinelli (UNIURB), J. Arduini (UNIURB), M. Maione (UNIURB), EYE-CLIMA: S. Eckhardt (NILU), Z. Klimont (IIASA), A. Stohl (UNIVIE), S. Platt (NILU)		
Internal reviewers	PARIS: J. Ovadnevaite (NUIG, WP Lead), S. Walter (UU) EYE-CLIMA: R. Thompson (NILU)		
Version: 1.0			

Horizon Europe Cluster 5: Climate, energy and mobility

"This project has received funding from the European Union's Horizon Europe Research and Innovation programme under HORIZON-CL5-2022-D1-02 Grant Agreement No 101081430 - PARIS and the Grant Agreement No 101081395 – EYE-CLIMA".

Table of Content

1. Changes with respect to the DoA (Description of the Action)

Due to work coordination and alignment of deliverables with the sister project EYE-CLIMA, this deliverable was created to replace the initial milestone M29 – Inverse estimates of BC emissions for focus countries. The changes were implemented in the amended Grant Agreement.

This new Deliverable - Preliminary emissions of BC for Europe – is a joint deliverable between the PARIS and EYE-CLIMA projects (in PARIS, D7.4 and in EYE-CLIMA, D3.8).

2. Dissemination and uptake

The estimates of BC emissions from Europe will be made publicly available to the scientific community and the relevant stakeholders through publication in the scientific literature.

Furthermore, in PARIS, for the focus countries Ireland and Italy, as part of the inventory verification work carried out in WP 2, the results will be communicated to emission inventory compilers of the Informative Inventory Reports drawn up in the framework of the United Nations Economic Commission for Europe (UNECE) Convention on Long Range Transboundary Air Pollution (CLRTAP). This will enable collaboration with decision-makers in the environmental protection field. In EYE-CLIMA, the results will be used in the European synthesis report, D5.9.

3. Short Summary of results

The FLEXPART-FLEXINVERT inversion framework for BC has been set-up and a new log-normal error distribution capability, recently developed for FLEXINVERT, was successfully implemented in this deliverable. The estimates of eBC emissions were obtained using the FLEXPART-FLEXINVERT modelling framework, the inversion method based on harmonised atmospheric BC observations for selected European sites of the ACTRIS and EMEP network.

FLEXPART simulations and the harmonised eBC observations from AE-33 instruments and mass concentration calculations were provided by the partner project EYE-CLIMA.

4. Evidence of accomplishment

Section 4.3 of this document is a detailed description of the task results, reporting BC emission estimates for Europe for the year 2022 obtained through an inverse modelling approach.

4.1 Introduction | Background of the deliverable

BC is an important aerosol constituent that has strong positive radiative forcing and severe health impacts. In addition, BC reduces albedo when deposited on snow exacerbating the warming effect. BC is emitted by incomplete combustion of fossil fuels and biomass. A comprehensive BC emission inventory is needed for a good understanding of the radiative forcing and associated climate feedback. It is also critical to minimise the very large uncertainty in the climate influence of BC.

In this deliverable, we aim to report a top-down observation-informed estimate of European BC emissions for 2022.

4.2 Scope of the deliverable

While the use of the FLEXPART-FLEXINVERT framework has been reported before, in this deliverable, the log-normal distribution method for prior flux errors was tested and implemented for the first time for BC.

Log-normal error distribution is more natural for log-normally distributed emissions such as BC. It also constrains posterior estimates to a positive value. This deliverable aims to test this implementation and pave the path for the final deliverable of BC estimates for the European domain.

4.3 Content of the deliverable

4.3.1 Methodology

4.3.1.1 Observation network

The harmonised BC atmospheric concentration data were provided by the collaborators from the EYE-CLIMA project. The following steps were involved for obtaining, processing, and harmonisation of the measurements.

Aerosol absorption coefficient (B_{abs}) data measured by 7-wavelength filter absorption photometers (Magee, AE33) were downloaded mostly via the EBAS data portal (https://ebas.nilu.no) or by correspondence.

As a quality control step, measurement data for all sites were screened for the correlation of ln(B_{abs}) vs ln(wavelength), with observations having R^2 less than 0.99 removed. Note that the ln(B_{abs}) vs ln(wavelength) fits typically have very high R^2, such that R^2=0.99 is below the 99th percentile, meaning this quality control measure normally removed less than 1% of data. The exceptions to this were remote sites such as Zeppelin, which had very low levels.

Conversion to equivalent black carbon (eBC) measured at B_{abs}=880 nm was done using mass absorption cross sections (MAC) derived from co-located filter-based measurements of elemental carbon (EC), where possible, or using the default instrument setting of MAC=7.77 g m^{-2}: eBC=B_{abs}/EC.

The observation stations used for the year 2022 are listed in Table 1, and their geographical locations are presented in Fig. 1a.

Table 1. Details of the observation sites used in the inversions for the year 2022.

Station code	Station name	Latitude	Longitude	Altitude asl (m)
C02	Payern	46.81	6.94	493.00
C05	Rigi	47.07	8.46	1035.00
D43	Hohenpeissenberg	47.80	11.02	975.00
E21	Madrid	40.46	-3.72	673.00
F27	Villeneueve d'Ascq	50.61	3.14	90.00
G01	Birmingham	52.46	-1.93	146.00
G00	Finokalia	37.99	23.82	280.00

I10	University College Dublin	53.31	-6.22	35.00
I26	Rome Villa Ada	41.93	12.51	64.00
N02	Birken II	58.39	8.25	219.00
N42	Zeppelin	78.91	11.89	475.00
S21	Hyltemossa	56.10	13.42	145.00
N73	Røros, Norway	59.92	10.77	27.40
F96	Lapland	67.97	24.12	572.00

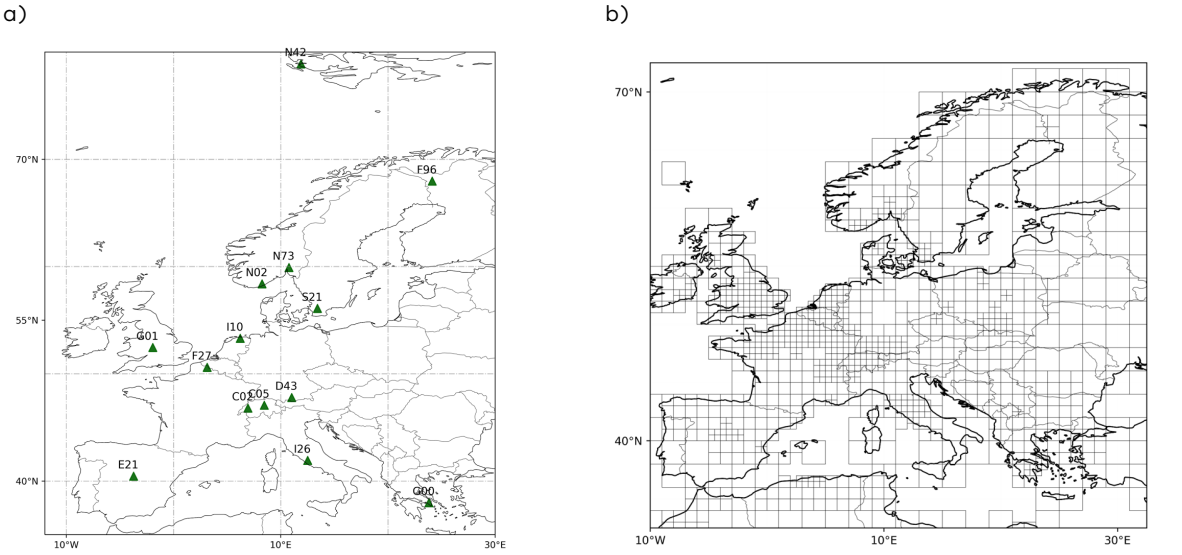

Fig. 1: a) The locations of the BC measurement stations used in the inversions; **b)** the inversion domain and the optimisation grid used based on the sensitivity of the observation network

4.3.1.2 Source–receptor relationships

The FLEXible PARTicle (FLEXPART) (Bakels et. al, 2024), a Lagrangian Particle Dispersion Model, was used to simulate atmospheric transport. The FLEXPART model was driven by the ECMWF (ERA5) meteorological fields with 137 vertical levels and a horizontal resolution of 0.5° × 0.5°. 50,000 spherical particles were released for each observation and tracked for 30 days backwards in time.

The wet-scavenging coefficients in FLEXPART for below-cloud scavenging by snow (Csnow) and rain (Crain) were set at 1. For in-cloud scavenging, the efficiency of aerosols to serve as cloud condensation nuclei (CCNeff) and ice nuclei (INeff) were set at 0.89 and 0.1, respectively.

4.3.1.3 Prior emissions

In this study, the following three BC emission inventories were used as priors:

- LRTAP baseline 2020 (Klimont et. al., 2023)
- ECLIPSE v6b 2020 (Klimont et. al., 2017)
- EDGAR HTAP v3 (Crippa et. al, 2023)

These inventories do not include emissions from wildfires. Hence, CAMS Global Fire Assimilation System (GFAS) 2022 biomass burning and vegetation fire emissions were added. GFAS utilises satellite observations of fire radiative power (FRP) to provide near-real-time information on the location and relative intensity of fires, to give an estimate of biomass burning and vegetation fire emissions.

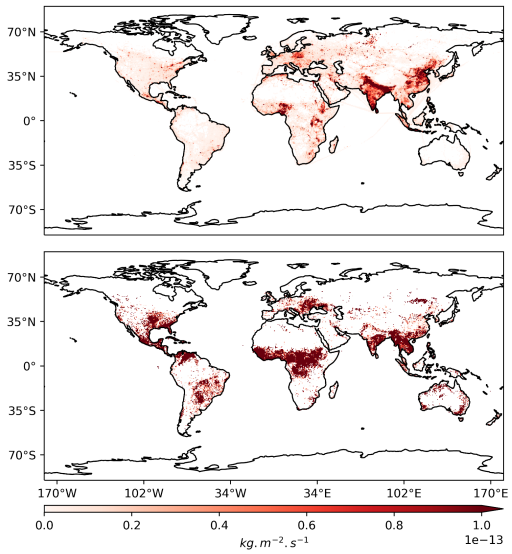

Fig. 2: LRTAP BC emission flux after removing the AWB sector (top) and the GFAS fire emissions (bottom) for March. The sum of these two fields makes the LRTAP prior.

To avoid double counting the agricultural waste burning (AWB) emissions, the AWB sector was removed and the GFAS fire emissions were added. The nearest available year for LRTAP and ECLIPSE inventories is 2020. For EDGAR HTAP, 2018 emissions were used. The global emissions flux for LRTAP in March 2020 and GFAS in March 2022 are shown in Fig. 2. To reduce the inversion state vector, an optimised inversion grid was prepared based on sensitivity maps from the transport model and prior emissions, as shown in Fig. 1b.

4.3.1.4 Sensitivity tests

Several sensitivity tests were conducted using different prior emissions, observation selection criteria, and inversion parameters.

LRTAP, ECLIPSE, and HTAP priors were used to assess the impact of prior emissions. In one of the sensitivity tests, an aseasonal prior, which remained constant throughout all months, was employed. For this, the January ECLIPSE emissions were used. To avoid periods when the boundary layer height and local transport dynamics could introduce inaccuracies into the transport model an observation selection criteria was used. For mountainous stations, observations recorded within a time window from 06:00 to 09:00 local time (LT) were used, and for non-mountainous sites, the time window was set from 12:00 to 15:00 LT. In one of the simulations, urban stations like Madrid (E21) and Dublin (I10) were removed to avoid high posterior emissions due to local pollution sources. In addition, inversion parameters such as prior flux error (*flxerr*) were varied from 50% to 100%, and observation error (*obserr*) from 20 to 100 ng m^{-3}. Table 2 lists all the sensitivity tests performed.

Moreover, a Monte Carlo ensemble of 20 inversions was performed to estimate uncertainties in the posterior estimates.

Table 2: Overview of all the inversion configurations used in the sensitivity tests.

Test	Prior	Obs selection	*flxerr*	*obserr*	no. of obs
1	ECLIPSE (Aseasonal)	All Obs	100	20	29742
2	ECLIPSE	All Obs	100	50	29742
3	ECLIPSE	Excluded Urban stations	100	100	25137
4	ECLIPSE	Selection criteria	100	100	6436

5	LRTAP	Selection criteria	100	100	6436
6	HTAP	Selection criteria	100	100	6436
7	ECLIPSE	Selection criteria	50	100	6436
8	ECLIPSE	Selection criteria	100	50	6436

4.3.2 Results and Discussion

Comparisons among prior and posterior emissions for the sensitivity tests concerning different priors and observation selection criteria are shown in Fig. 3. The monthly prior and posterior emissions exhibited a clear seasonal pattern, with emissions peaking during winter.

Fig. 3a highlights that the posterior estimates are influenced by the choice of prior emission inventory. However, changes in observation selection criteria (Fig. 3b) and inversion parameters such as *flxerr* and *obserr* showed limited sensitivity to the posterior estimates. In addition, all posterior estimates showed unexpectedly higher emissions in March compared to the other months.

The spatial distribution of differences between the posterior and the prior emission fluxes are presented for each month for LRTAP prior (Fig. 4); comparisons with ECLIPSE showed similar patterns. Regions with emission differences between the posterior and LRTAP prior emissions are identified in Fig. 4. In particular, for March significant increases in emission flux are observed in the east-central European region compared to the prior. During the winter months, BC emissions in north-central Europe are overestimated by the LRTAP (Fig. 4) and ECLIPSE (not shown) priors. In contrast, emissions from Great Britain are consistently underestimated by these inventories across all months except January.

Monthly and annual emissions from the total domain and the top five emitting countries—Poland, France, Italy, Spain, and Great Britain—are shown in Table 3.

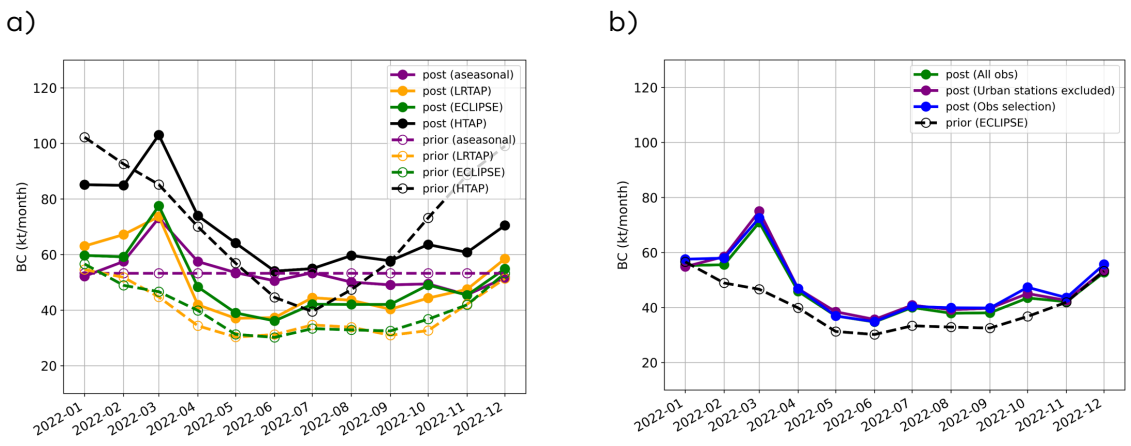

Fig. 3: Comparisons among (a) prior (dotted lines) and posterior emissions (solid lines) for different prior emission inventories, and (b) posterior emission estimates for different observation selection criteria.

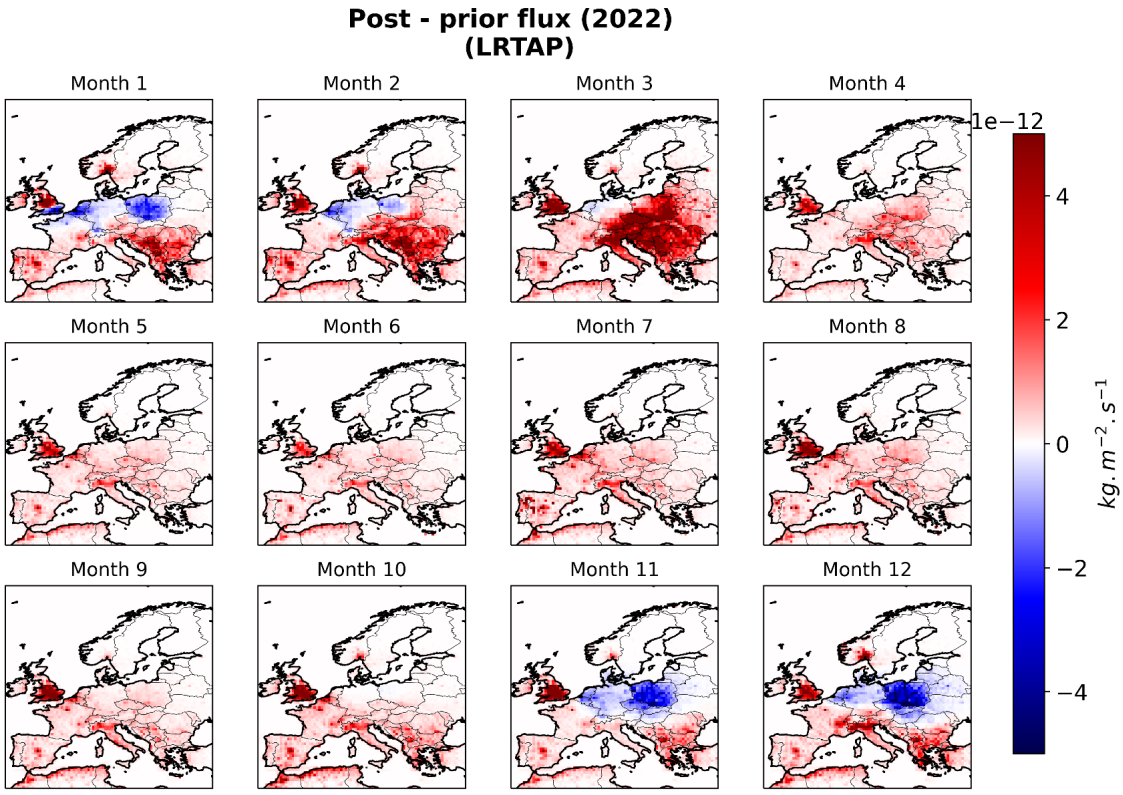

Fig. 4: Difference between the posterior and the LRTAP prior emission fluxes for each month in 2022.

Table 3: Monthly BC inversion estimates for the top 5 emitting countries and the total domain (in kt/month). The uncertainties in brackets represent the 10th and 90th percentiles.

Month	Poland	France	Italy	Spain	Great Britain	Total Domain
JAN	5.16 (4.22, 6.49)	3.69 (2.85, 4.42)	2.92 (2.37, 3.43)	2.56 (1.84, 3.15)	2.76 (2.23, 3.34)	65.08 (55.16, 75.74)
FEB	6.03 (4.09, 7.53)	4.38 (3.61, 5.24)	3.31 (2.52, 4.06)	3.16 (1.97, 4.23)	2.46 (1.28, 3.38)	67.21 (57.41, 81.89)
MAR	9.07 (7.07, 11.6)	5.19 (3.81, 6.97)	4.9 (3.47, 6.3)	2.84 (1.72, 3.8)	2.96 (1.78, 3.9)	85.23 (72.07, 104.04)
APR	3.98 (2.26, 5.56)	3.75 (1.98, 5.55)	2.59 (1.65, 4.66)	1.87 (1.04, 3.09)	1.84 (0.96, 3.1)	54.59 (44.91, 65.69)
MAY	2.99 (1.8, 4.78)	3.41 (2.51, 4.7)	2.43 (1.54, 3.4)	2.02 (1.24, 3.03)	1.61 (0.99, 2.4)	45.57 (36.94, 54.44)
JUN	2.55 (1.45, 3.52)	3.1 (2.4, 4.01)	2.31 (1.32, 3.27)	2.09 (1.42, 2.99)	1.22 (0.79, 1.88)	42.29 (35.45, 50.93)
JUL	2.63 (1.93, 3.31)	3.82 (2.64, 4.86)	2.6 (1.73, 3.6)	2.35 (1.52, 3.24)	1.44 (0.89, 1.84)	49.3 (39.92, 58.34)
AUG	2.65 (1.65, 4)	3.32 (2.57, 4.55)	2.33 (1.57, 3.05)	2.24 (1.36, 3.23)	1.84 (1.01, 2.82)	46.04 (37.96, 52.98)
SEP	2.5 (1.81, 3.34)	3.21 (2.25, 4.59)	2.13 (1.46, 2.9)	2.01 (1.32, 2.98)	2.07 (1.11, 3.31)	47.01 (37.46, 57.89)
OCT	3 (1.92, 4.5)	3.17 (2.31, 3.82)	2.15 (1.39, 2.88)	2.49 (1.58, 3.61)	2.28 (1.25, 3.52)	52.81 (44.09, 60.59)
NOV	2.73 (2.31, 3.42)	3 (2.31, 3.72)	2.24 (1.46, 3.33)	2.16 (1.46, 2.92)	2.84 (1.3, 4.04)	50.65 (43.31, 59.31)
DEC	3.44 (2.65, 4.37)	4.83 (3.33, 6.3)	3.89 (2.74, 5.86)	2.59 (1.73, 3.34)	2.22 (1.24, 3.07)	61.76 (52.41, 70.37)
Total	46.73	44.87	33.8	28.38	25.54	667.54

For the countries where posterior emissions were significantly higher than prior emissions in March, the monthly trend of burnt area (Fig. 6) and the supply and transformation of fossil fuels (Fig. 7) were investigated as proxies for BC emissions from the combustion of biomass and fossil fuels, respectively.

The highest number of fires during the spring fire season in 2022 was recorded in several east-central European countries, including Austria, Hungary, Poland, and Slovakia, primarily due to extreme drought, as documented in the annual report on Forest Fires in Europe (San-Miguel-Ayanz et al., 2022). The monthly inversion estimates and weekly trends of burned areas for selected European countries in 2022 are shown in Fig. 5 and Fig. 6, respectively.

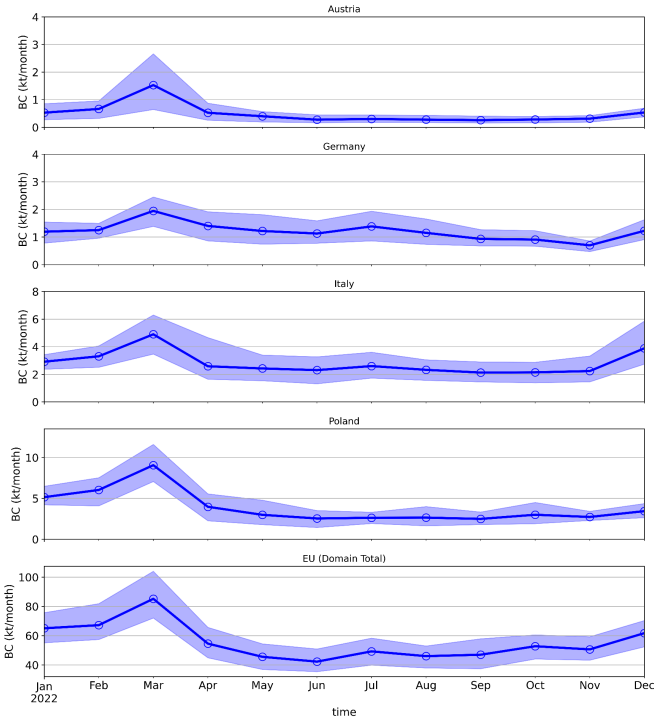

Fig. 5: Monthly inverse emission time series for the countries in the east-central part of the domain (a) Austria, (b) Germany, (c) Italy, (d) Poland that showed higher emissions in March, and (e) the whole domain. The average a posteriori emissions across all the inversions performed are represented by the solid blue line, while the shaded regions indicate uncertainty ranges defined by the 10th and 90th percentiles.

Among the selected European countries with a higher increase in posterior emissions in March, the largest burned area was recorded in Italy (58,751 ha), followed by Germany (4,293 ha), Austria (1,016 ha), and Poland (465 ha). In Austria, Poland, and Germany, most of the fire-affected areas were recorded in March. In Italy, fire-affected areas were observed between January and October, with the majority of burned areas occurring between June and September.

The year 2022 was also affected by the escalation of the conflict in Ukraine in February 2022, which raised new concerns about the EU's energy security. Countries such as Italy, Hungary, Slovakia, Romania, and the Netherlands were dependent on Russian-imported natural gas as the primary source of energy (Cebotari, 2022). It was reported by Aghaei et al. (2024) that increased biomass burning for residential heating in Milan (Italy) occurred as a result of the Russia-Ukraine war, leading to higher PM2.5 levels. Similar effects could have been observed in other parts of Italy and the EU, resulting in higher biomass usage during cold periods.

March was among the months with the highest supply and transformation of (brown + hard) coal in Germany (Fig. 7b) and Poland (Fig. 7d), as well as oil and petroleum products in Austria (Fig. 7a) and Italy (Fig. 7c). In Austria (Fig. 7a), January was recorded as the month with the highest supply and transformation of brown and hard coal, with values ranging from 9% to 26.6% higher compared to the other months in 2022.

Furthermore, the supply and transformation of oil and petroleum products was reported to be up to 22.5% higher in March, May, and September compared to the other months in 2022. In Germany (Fig. 7b), the supply and transformation of brown coal was between 2.2% and 34.4% higher in March than in the other months in 2022. Additionally, the supply and transformation of brown and hard coal were up to 24% higher in March and November compared to the other months in 2022. In Italy (Fig. 7c), the supply and transformation of hard coal were highest in July, with values ranging from 3.9% to 58.8% higher than in the other months in 2022. Additionally, the supply and transformation of oil and petroleum products was up to 22.7% higher in March and from July to October compared to the other months in 2022. In Poland (Fig. 7d), the supply and transformation of brown and hard coal were between 3.6% and 23.2% higher in March compared to the other months in 2022.

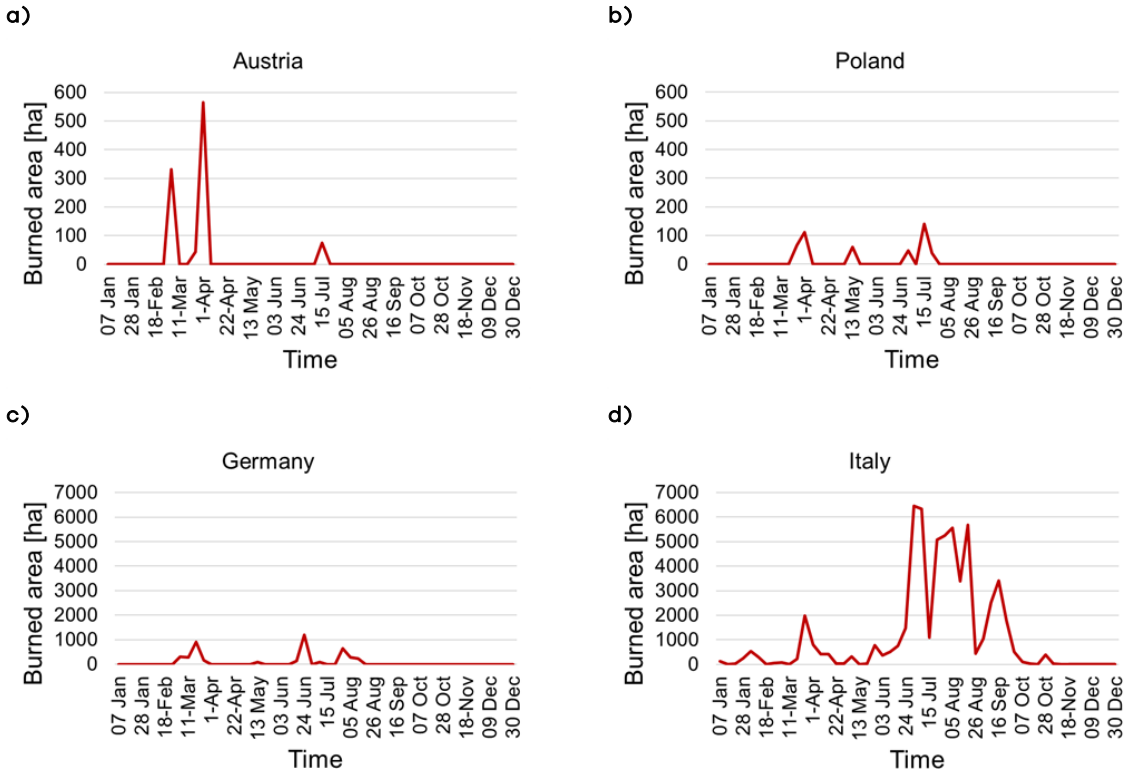

Fig. 6: Weekly burned areas in a) Austria, b) Poland, c) Germany, and d) Italy of the fires mapped in the European Forest Fire Information System.

Available at https://forest-fire.emergency.copernicus.eu/apps/effis.statistics/seasonaltrend (accessed on 29 January 2025).

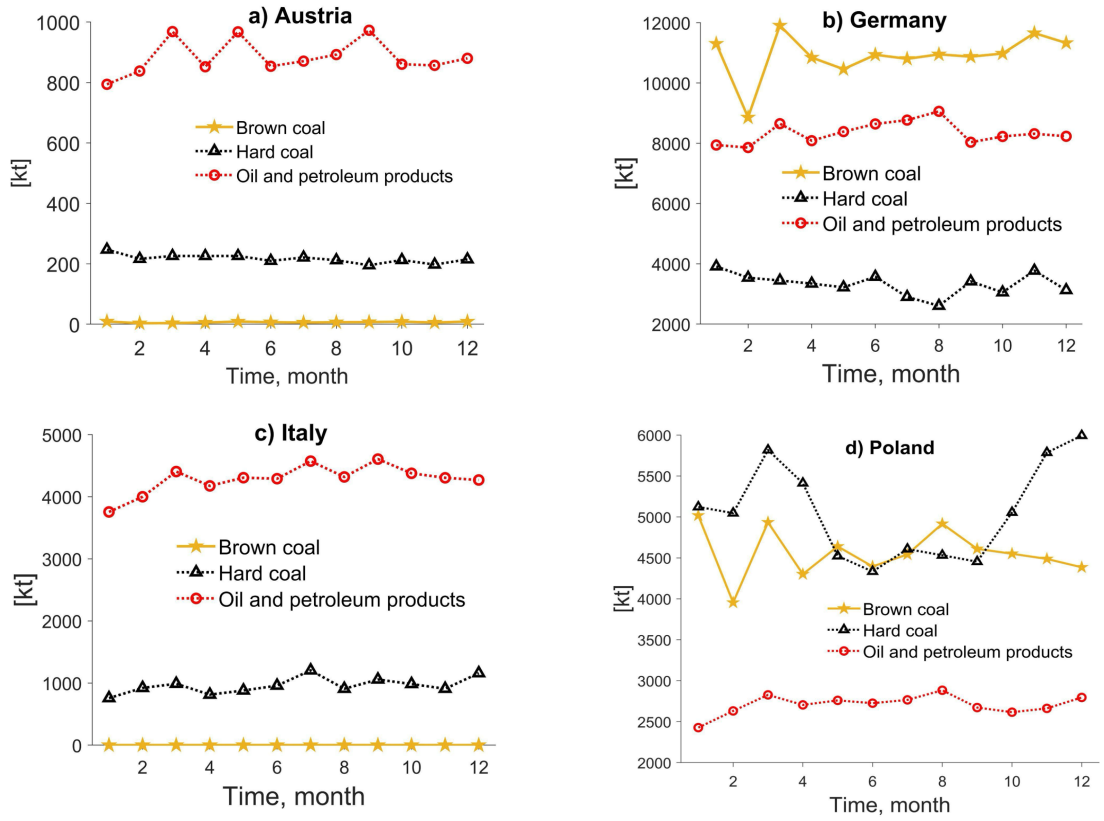

Fig. 7: Monthly supply and transformation of solid fossil fuels, oil, and petroleum products in a) Austria, b) Germany, c) Italy, and d) Poland in 2022. Own elaboration based on data from Eurostat [nrg_cb_sffm__custom_15184772], [nrg_cb_oilm__custom_15187565].

4.4 Conclusion and possible impact

This study estimates monthly BC emissions from the European continent for the year 2022 using inverse modelling. Comparisons between inversion estimates and bottom-up emission inventories showed differences both in the temporal and spatial distribution of BC emissions, especially in north-central Europe and Great Britain. The inverse estimates confirm seasonal patterns with emissions peaking in winter, as seen in the prior inventories.

However, the inverse estimates revealed significantly higher emissions in March 2022 in north-central Europe. To investigate the potential causes of the differences in BC emissions, we examined wildfires and fossil fuels as potential contributing factors. Extreme droughts during the spring fire season in this region led to a surge in wildfires.

Additionally, there was a notable increase in the supply and transformation of brown and hard coal to the EU during this period. The Russia-Ukraine conflict, which resulted in sanctions on natural gas and oil imports to European countries, may have also contributed to this effect. These factors likely contributed to the high BC emissions in March 2022, and a more detailed analysis should be conducted in the future.

Our results reiterate the importance of inverse modelling methods, especially in unprecedented periods with geopolitical or natural influences that are difficult to capture with statistical methods.

4.5 References

Aghaei, Y., Badami, M. M., Tohidi, R., Subramanian, P. G., Boffi, R., Borgini, A., ... & Sioutas, C. (2024). The Impact of Russia-Ukraine geopolitical conflict on the air quality and toxicological properties of ambient PM2. 5 in Milan, Italy. Scientific reports, 14(1), 5996.

Bakels, L., Tatsii, D., Tipka, A., Thompson, R., Dütsch, M., Blaschek, M., ... & Stohl, A. (2024). FLEXPART version 11: Improved accuracy, efficiency, and flexibility. Geoscientific Model Development, 17(21), 7595-7627.

Cebotari, L. (2022). Ukraine crisis: The trigger for the EU to cut its dependence on Russian fossil fuels. R. Pamfilie, V. Dinu, C. Vasiliu, D. Pleșea, L. Tăchiciu eds, 733-740.

Crippa, M., Guizzardi, D., Butler, T., Keating, T., Wu, R., Kaminski, J., Kuenen, J., Kurokawa, J., Chatani, S., Morikawa, T., Pouliot, G., Racine, J., Moran, M. D., Klimont, Z., Manseau, P. M., Mashayekhi, R., Henderson, B. H., Smith, S. J., Suchyta, H., Muntean, M., Solazzo, E., Banja, M., Schaaf, E., Pagani, F., Woo, J.-H., Kim, J., Monforti-Ferrario, F., Pisoni, E., Zhang, J., Niemi, D., Sassi, M., Ansari, T., and Foley, K.: The HTAP_v3 emission mosaic: merging regional and global monthly emissions (2000–2018) to support air quality modelling and policies, Earth Syst. Sci. Data, 15, 2667–2694, doi:10.5194/essd-15-2667-2023, 2023.

Klimont, Z., Heyes, C., Rafaj, P., Hoglund-Isaksson, L., Purohit, P., Kaltenegger, K., Gomez-Sanabria, A., Kim, Y., Winiwarter, W., Warnecke, L., Schoepp, W., Lindl, F., Kiesewetter, G., Sander, R., & Nguyen, B. (2023). Global gridded anthropogenic emissions of air pollutants and methane for the period 1990-2050 [Data set]. Zenodo. https://doi.org/10.5281/zenodo.10366132

Klimont, Z., Kupiainen, K., Heyes, C., Purohit, P., Cofala, J., Rafaj, P., ... & Schöpp, W. (2017). Global anthropogenic emissions of particulate matter including black carbon. Atmospheric Chemistry and Physics, 17(14), 8681-8723.

San-Miguel-Ayanz, J., Durrant, T., Boca, R., Maianti, P., Liberta`, G., Jacome Felix Oom, D., Branco, A., De Rigo, D., Suarez-Moreno, M., Ferrari, D., Roglia, E., Scionti, N., Broglia, M., Onida, M., Tistan, A. and Loffler, P., Forest Fires in Europe, Middle East and North Africa 2022, Publications Office of the European Union, Luxembourg, 2023, doi:10.2760/348120, JRC135226.

5. History of the document

Version	Author(s)	Date	Changes
1	Saurabh Annadate	31/01/2025	First draft
	Enrico Mancinelli	31/01/2025	First draft
	Michela Maione	31/01/2025	First draft
	S. Walter	20 February 2025	First check, re-send to distribution EYE-CLIMA
	Rona Thompson	25/02/2025	Minor corrections
	Sabine Eckhardt	28/02/2025	Minor corrections